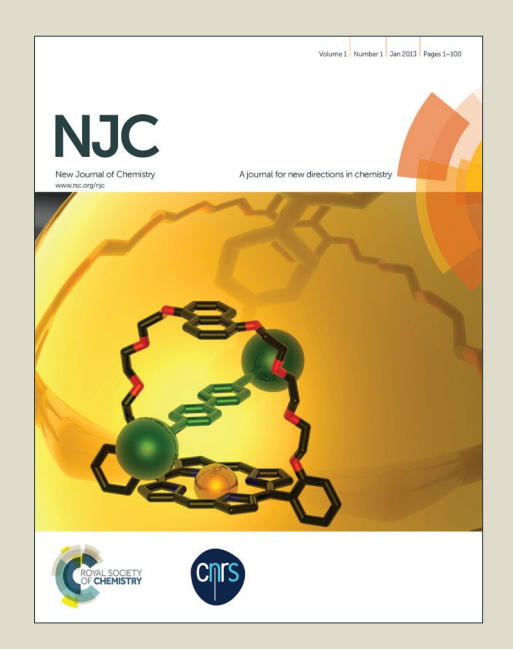
NJC

Accepted Manuscript



This is an *Accepted Manuscript*, which has been through the Royal Society of Chemistry peer review process and has been accepted for publication.

Accepted Manuscripts are published online shortly after acceptance, before technical editing, formatting and proof reading. Using this free service, authors can make their results available to the community, in citable form, before we publish the edited article. We will replace this Accepted Manuscript with the edited and formatted Advance Article as soon as it is available.

You can find more information about *Accepted Manuscripts* in the **Information for Authors**.

Please note that technical editing may introduce minor changes to the text and/or graphics, which may alter content. The journal's standard <u>Terms & Conditions</u> and the <u>Ethical guidelines</u> still apply. In no event shall the Royal Society of Chemistry be held responsible for any errors or omissions in this *Accepted Manuscript* or any consequences arising from the use of any information it contains.



Journal Name

RSCPublishing

ARTICLE

wwwCite this: DOI: 10.1039/x0xx00000x

Received 00th January 2012, Accepted 00th January 2012

DOI: 10.1039/x0xx00000x

www.rsc.org/

CO gas sensing properties of direct-patternable SnO₂ films containing graphene or Ag nanoparticles

Hyuncheol Kim, Chang-Sun Park, Kyung-Mun Kang, Min-Hee Hong, Yong-June Choi, Hyung-Ho Park*

The gas sensing properties of direct-patternable SnO_2 thin films prepared by photochemical solution deposition were improved by an incorporation of graphene or Ag nanoparticles. The CO gas sensitivity of the SnO_2 thin film was 3.65, but increased to 6.84 and 18.06 with graphene and Ag nanoparticles incorporation, respectively. Direct-patterning of graphene or Ag nanoparticles incorporated SnO_2 thin films can be performed to a 40 μ m scale pattern without a photoresist or etching process.

Introduction

Tin dioxide (SnO₂) thin films have been increasingly studied as transparent electrode materials for display devices and anode materials for gas sensors due to the high optical transparency, high chemical durability, and low cost.¹⁻⁴ Gas sensors based on a metal oxide semiconductor have attracted considerable attention because of their low cost, high sensitivity, and high compatibility with microelectronic processing. CO gas detection can be attributed to a surface reaction, which occurs at lower temperatures (< 500°C).⁵ When O₂ molecules are adsorbed to the surface of a SnO₂ thin film, they trap the electrons in the form of ions. Alternatively, when a gas sensor is exposed to CO gas, CO is oxidized by O⁻ and releases electrons to the surface. O⁻ is believed to become dominant at operating temperatures of 300-450°C.⁶

There have been many efforts to modify and improve the material properties by the applied nanostructure and the addition of nanosized materials.^{7, 8} Ag nanoparticles have been widely used in gas sensor applications and their incorporation into materials basically relies on the ability in acting either as electron sink or redox catalyst. 9, 10 Furthermore Ag metal dopant in SnO₂ gas sensor has been reported acting with a catalytic effect. The metal additive acts as a catalyst to modify the surface reactions of metal oxide semiconductors toward sensing gases.¹¹ In particular, it is reported that the noble metal acts as a strong acceptor of electrons and remove electrons from the oxide. So, the metal oxide has large response. 12 Graphene has very high mobility ($\sim 200.000 \text{ cm}^2/\text{Vs}$) with π -bonding on the surface and good potential for detecting gases due to their large surface area resulting from a large aspect ratio and outer walls. 13, 14 Also, the graphene has been reported that the potential barrier of oxide could be changed by making the hetero-junctions at the interface of oxide. Therefore, an

improvement in the sensor response in the case of hybrid graphene—oxide was expected. 15

A micro-patterning process is commonly used for the fabrication of gas sensor devices. ¹⁶ The conventional etching process is accompanied by the generation of physical defects and the resulting degradation of properties, pollution from hazardous materials, and additional outcomes. Photoresists and etching are not necessary when using photochemical solution deposition because the coated films behave like a negative photoresist. As a result, damage and problems from conventional etching can be avoided. ¹⁷

The effects of graphene or Ag nanoparticles on the gas sensing properties of SnO_2 thin films were investigated in this study. The gas sensitivity of SnO_2 sensors was improved through incorporation of graphene or Ag nanoparticles. Furthermore, direct-patterning of SnO_2 thin films containing graphene or Ag nanoparticles was achieved using a photosensitive solution and ultra violet (UV) light exposure to avoid damage from dry etching and simplify the micro-scaled patterning procedure.

Results and discussion

The direct-patterning of SnO_2 thin film containing graphene or Ag nanoparticles was examined by removing the area not exposed to UV using 4-methyl-2-pentanone. In the scanning electron microscopy (SEM) image of Figure 1, the relatively bright area corresponds to the SnO_2 thin film with incorporated Ag nanoparticles and the dark area is the Si substrate. As shown at the pattern edge, patterning at a scale of several tens of microns was successfully obtained by lithography using photochemical solution deposition. The graphene-incorporated, SnO_2 thin film also showed the same behavior.

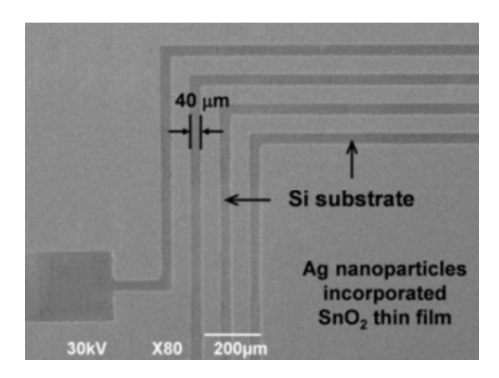


Figure 1. SEM image of SnO₂ thin film with incorporated direct-patterned Ag nanoparticles annealed at 500°C.

X-ray diffraction patterns of SnO₂ thin films containing graphene or Ag nanoparticles annealed at 500°C are presented in Figure 2. The diffraction patterns were indexed as (110), (101), (200), (211), and (220) peaks of the cassiterite crystalline SnO₂ phase.¹⁸ Similar diffraction patterns were observed after the incorporation of graphene or Ag nanoparticles. The presence of graphene or Ag nanoparticles did not significantly affect the phase formation of SnO₂, but the diffraction pattern intensity decreased due to the degraded crystalline state of SnO₂ with graphene or Ag nanoparticles compared to the pristine SnO₂. The presence of graphene or Ag nanoparticles potentially increased the impurity content in the SnO₂ thin films and may act as a grain growth inhibitor.

The surface morphology change of the SnO₂ according to the addition of Ag nanoparticles and graphene was analyzed using AFM, and the results are presented in Fig. 3. As shown in Figure 3, the surface roughness of the graphene-incorporated SnO₂ thin film was approximately 3.7 times greater than that of the pristine SnO₂ thin film. The AFM results conclude that the bumps were formed by graphene incorporation and they increased the surface area of the films. The larger surface area allows more gas molecules to be absorbed to the surface of the sensing film.

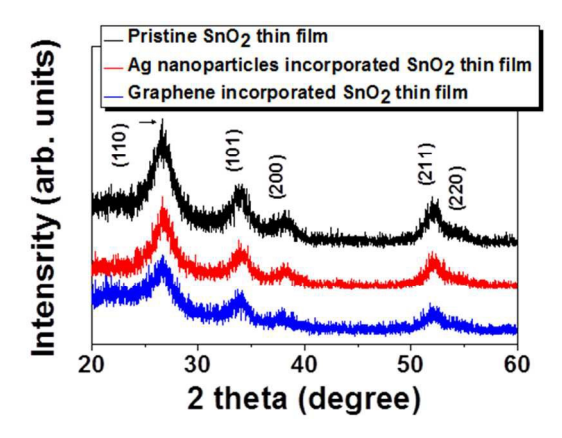


Figure 2. XRD patterns of pristine SnO_2 and SnO_2 hybrid films annealed at 500°C with 0.0055 wt.% Ag nanoparticles and 0.05 wt.% graphene.

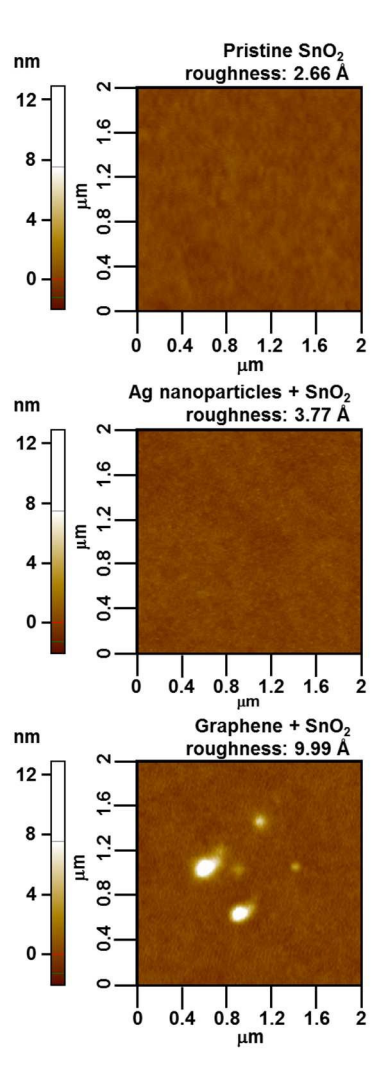


Figure 3. AFM images of pristine SnO₂ and SnO₂ hybrid films annealed at 500°C with 0.0055 wt.% Ag nanoparticles and 0.05 wt.% graphene.

The chemical bonding states of SnO₂ thin films containing graphene or Ag nanoparticles were examined using XPS to investigate the change of chemical bonding states. The films were prepared by annealing at 450°C for 12 h under air (oxidation) and vacuum (reduction) ambient. C 1s, O 1s, Sn 3d, and Ag 3d core levels were obtained and the results of O 1s and Sn 3d are given in Figure 4. However Ag 3d_{5/2} peak was not observed due to an undetectable small amount of Ag NPs in SnO₂ film.¹⁹ In C 1s spectrum of SnO₂ thin film containing graphene, no extra peak contribution from graphene was observed due to its small amount as the case of Ag NPs or almost same binding energy between graphene and air contaminated hydrocarbon. ^{20,21} The binding energies of the core level were corrected using the reference C 1s peaks at 284.5 eV.22 Changes in the core level spectra of Sn 3d and O 1s would indicate a formation of SnO₂ between Sn and O atoms. As shown in Figure 4a, the binding energy of the O-Sn bond in the films annealed at air ambient was the same.

Journal Name

(a) Air ambient Vacuum ambient

| Signature | Signatur

Figure 4. XPS spectra of (a) O 1s and (b) Sn 3d core levels of pristine SnO₂ and SnO₂ hybrid films with 0.0055 wt.% Ag nanoparticles and 0.05 wt.% graphene after annealing at 450°C under air and vacuum ambient.

Binding Energy (eV)

However, in the case of the films annealed at vacuum ambient, the binding energy of the SnO_2 thin film containing Ag nanoparticles was less than those of the pristine SnO_2 and graphene-incorporated SnO_2 thin films.

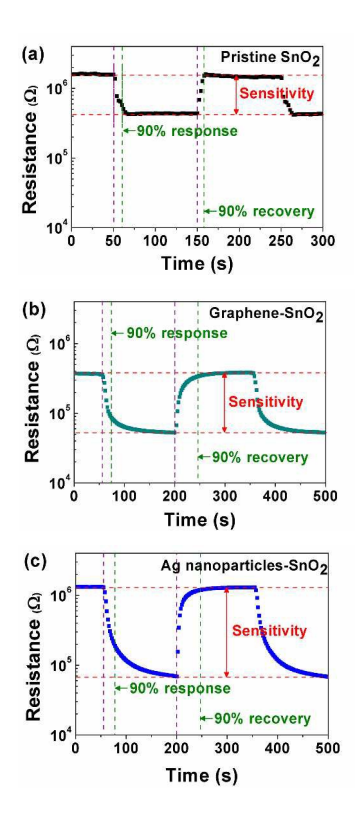


Figure 5. Transient response of (a) pristine SnO₂, (b) SnO₂ with incorporated Ag nanoparticles, and (c) graphene-incorporated SnO₂ thin film sensor containing Ag nanoparticles and graphene measured at 400°C with 100 ppm CO gas.

Additionally, as shown in Figure 4b, the binding energy of the Sn 3d core level spectra exhibited similar behavior to those of the O 1s spectra. Based on these results, the x of SnO_{2-x} increased by incorporation of the Ag nanoparticles. Usually, noble metals inject electrons in the conduction band of the metal oxide by changing the oxidation state of noble metal as per following reaction.²³

$$metal^{y+} + xVO^{\bullet} \leftrightarrow metal^{(y-x)+} + xVO^{\bullet \bullet}$$

Where VO* the singly ionized oxygen vacancy, and VO* is the doubly ionized oxygen vacancy. Therefore, the film was more reduced and the oxygen vacancies increased. Nonstoichiometric SnO₂ can be characterized with oxygen vacancies, which are a cause of the conduction mechanism in SnO₂. ^{24, 25}

Hence the gas sensing analyses were carried out to clarify the effect of changed surface area and state of SnO₂ due to the Ag nanoparticles and graphene, and the results are given in Fig. 5. During exposure to 100 ppm CO at 400°C, the sensor resistance decreased, which indicates that the SnO₂ thin films were an n-type semiconductor sensor. From the difference between the sensor resistance in air (Rair) and the sensor resistance in CO (R_{CO}), the sensitivity of the sensors (sensitivity = R_{air} / R_{CO}) can be predicted.²⁶ The sensitivity of the SnO₂ sensor with incorporated nanostructure (graphene or Ag nanoparticles) was greater than that of the pristine SnO₂ sensor because the difference between R_{air} and R_{CO} increased compared to the pristine SnO₂ sensor, as shown in Figure 6a. Sensing properties, such as sensitivity, 90% response time, and 90% recovery time of the nanostructure-incorporated SnO₂ sensor, were shown in Figure 6b and measured as 3.65, 10.04, and 7.04 s, respectively. The sensitivities of the SnO₂ containing graphene or Ag nanoparticles sensors increased to 6.84 or 18.06, respectively.

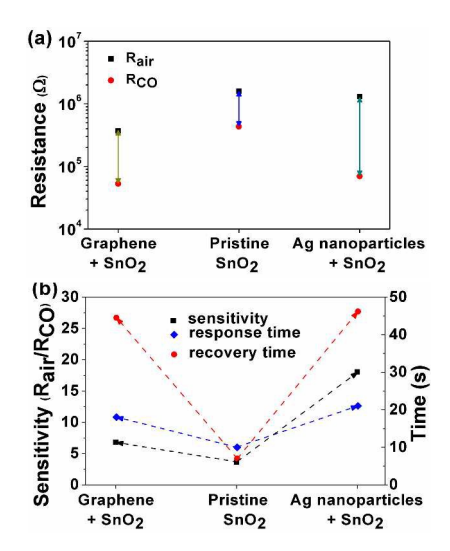


Figure 6. (a) Sensor resistance of nanostructure-incorporated SnO_2 sensor in dry air and 100 ppm CO balanced with dry N_2 , (b) sensitivity (\blacksquare), 90% response time (\bullet), and 90% recovery time (\bullet) of nanostructure-incorporated SnO_2 sensors measured at 400°C in dry air and 100 ppm CO balanced with dry N_2 .

SnO₂ thin films have lower R_{CO} and higher R_{air} as they were oxidized in air and reduced in CO gas. The R_{CO} of sensors containing graphene or Ag nanoparticles decreased more than a pristine SnO₂ sensor. Ag nanoparticles and graphene decreased resistivity of the SnO₂ thin films as shown in previous works.²⁷ ²⁸ When the air flowed, SnO₂ thin film was oxidized by the oxygen in air and the resistance increased. Although the nanostructure-incorporated SnO₂ sensor was also oxidized, the difference between R_{CO} and R_{air} increased more than those of the pristine SnO₂ sensor. This difference was due to the surface area increased by the graphene or oxygen vacancies formed by the Ag nanoparticles. The general gas sensing model is based on modulation of the depletion layer by oxygen absorption. In general, an incorporation of graphene induces an increase of electrical conductivity of metal oxides due to an enhancement of carrier mobility. However if the graphene exist on the surface, it will enhance the specific surface area and change the potential barrier of oxide. 13, 14 This is because in case of synthesis of material using solution process, the metal oxide will be wrapped with graphene on surface of interior oxide. As a result, the graphene has a large surface to volume ratio and the surface area of the film increased depending on graphene incorporation.²⁹ As an above effect, the graphene increases the absorption of oxygen ion and also the ratio of change of resistance of metal oxide. Therefore, the sensitivity of the graphene-incorporated SnO₂ sensor was increased despite low Rair. Ag nanoparticles generated oxygen vacancies in the SnO₂ matrix and the oxygen vacancies acts as reaction sites for oxygen in air. 30, 31 As a result, the Rair of SnO₂ sensor with incorporated Ag nanoparticles increased similarly to those of the pristine SnO₂ sensor. With the decreased R_{CO} and similar Rair, the SnO₂ sensor with incorporated Ag nanoparticles has more sensitivity than the pristine SnO2 and grapheneincorporated SnO₂ sensors. Because the sensor resistance changed due to the increase in electron concentration resulting from the oxidation and reduction reactions facilitated by the reaction gas, the response and recovery time increased with an increase in the difference between Rair and RCO. The increased response and recovery time would be expected for a sensor with highly fluctuating resistance, however, as shown in Figure 6b, the response and recovery times of the SnO₂ sensor with incorporated Ag nanoparticles were similar to the grapheneincorporated SnO₂ sensor despite a large difference in the sensitivity. Oxygen in air reacted easily on the SnO2 matrix in the SnO₂ sensor with incorporated Ag nanoparticles due to the oxygen vacancies formed by the Ag nanoparticles. From these reasons, oxidation and reduction occurring on the surface increased, making the movement of the surface electrons quite rapid. As a result, the sensitivity increase in the SnO2 sensor from oxygen vacancies for reduction and oxidation by Ag nanoparticle incorporation was more important than that from the larger surface area by graphene incorporation.

Conclusions

The CO gas-sensing behavior of a SnO₂ gas sensor with graphene or Ag nanoparticles incorporation was investigated. The presence of graphene or Ag nanoparticles does not affect the phase formation of SnO₂ films, but the film crystallinity was slightly degraded with the incorporation. The CO gas sensitivity was enhanced by the incorporation of Ag nanoparticles or graphene into the SnO₂ sensor. Graphene in the SnO₂ sensor increased sensitivity by increasing the surface area. However, the SnO₂ sensor with Ag nanoparticles showed increased sensitivity than that of the graphene incorporation because oxygen vacancies formed by Ag nanoparticles act as reaction sites for reduction and oxidation by oxygen.

Experimental

The photosensitive precursor for the production of SnO₂ films was tin 2-ethylhexanoate, $Sn(O_2CCH(C_2H_5)C_4H_9)_2$. The solvent and sol stabilizer were 4-methyl-2-pentanone and monoethanolamine, respectively. Tin 2-ethylhexanoate was dissolved in 4-methyl-2-pentanone at 0.3 monoethanolamine was added for stabilization at a molar ratio of 1.0. The dissolved photosensitive solution was stirred at room temperature. Ag nanoparticles were prepared by spontaneous reduction of Ag 2-ethylhexanoate in a dimethyl sulfoxide solvent. The concentration of Ag 2-ethylhexanoate was 1×10^{-4} M and trisodium citrate was used as a capping agent for formation of size-controlled Ag nanoparticles.³² Graphene (AO-2, Graphene Supermarket) was used as a graphene source. Graphene in the mixed solution was dispersed by a sonicator. 33 To obtain SnO₂ thin films containing graphene or Ag nanoparticles, a 0.05 wt.% graphene or 0.0055 wt.% Ag nanoparticles dispersed solution was added to the SnO₂ photosensitive solution. The graphene and Ag nanoparticles contents were selected by considering the atomic weight and percolation effect from previous works.^{27, 28} The solution was spin-coated at 2,000 rpm for 30 s on glass and Si substrates with Pt-interdigitated electrodes (IDE). For direct-patterning, the spin-coated film was exposed to 365-nm wavelength UV light. The UV exposed films were then washed with 4-methyl-2-pentanone to remove the unexposed area of the film. After washing, the films were aged at 50°C for 12 h in a dry oven and annealed at 500°C for 1 h in a tubular furnace under an O2 atmosphere to remove the solvent and organic residues. Finally, the films were annealed in a vacuum furnace at 450°C for 12 h. A sensor for CO gas was fabricated using a SiO₂/Si substrate with Pt IDE in which the gap between each electrode was 5 μm. The thickness of the Pt was 200 nm and the IDE patterns were fabricated using photolithography and dry etching. The responses of the fabricated gas sensors to CO gas were measured at 400°C by monitoring the change in sensor resistances while changing the flow gas from dry N2 to test gases (100 ppm CO balanced with dry N₂). To eliminate interfering effects, a constant flow rate of 1000 sccm for the dry air and test gases was used. The film resistance was measured under a DC bias voltage of 3 V using a source measurement **Journal Name**

unit (Keithley 2635A). The crystallinity was analyzed by an X-ray diffractometer (XRD, D/MAX-2000, Rigaku) with Cu K α radiation. The surface roughness and morphology of the films were analyzed in non-contact mode by atomic force microscopy (AFM, XE-100, Park Systems) with a baseline noise of 0.01 nm. X-ray photoelectron spectroscopy (XPS, K-Alpha, Thermo Scientific) was used with a monochromated Al K α source to investigate the surface chemical bonding state of the films. The accelerating voltage and emission current of the X-ray source were 15 kV and 20 mA, respectively.

Acknowledgements

This work was supported by a National Research Foundation of Korea (NRF) grant funded by the Korean government (MEST) (No. 2012R1A2A2A01011014).

Notes and references

Department of Materials Science and Engineering, Yonsei University, 50 Yonsei-ro, Seodaemun-gu, Seoul 120-749, Republic of Korea Fax: +82328655178; E-mail: hhpark@yonsei.ac.kr (H.-H. Park)

- V. V. Simakov, O. V. Yakusheva, A. I. Grebennikov, V. V. Kisin, Tech. Phys. Lett., 2005, 31, 339-340.
- K. L. Chopra, S. Major, D. K. Pandya, *Thin Solid Films*, 1983, 102, 1-46.
- 3. A. L. Dawar, J. C. Joshi, J. Mater. Sci., 1984, 19, 1-23.
- 4. A. Tiburcio-Silver, A. Sanchez-Juarez, *Mat. Sci. Eng. B-Solid* 2004, 110, 268-271.
- 5. O. Byl, J. T. Yates Jr., J. Phys. Chem. B 2006, 110, 22966-22967.
- C. Wang, L. Yin, L. Zhang, D. Xiang, R. Gao, Sensors, 2010, 10, 2088-2106.
- B. Wang, L. F. Zhu, Y. H. Yang, N. S. Xu, G. W. Yang, J. Phys. Chem. C, 2008, 112(17), 6643–6647.
- 8. N. Du, H. Zhang, X. Ma, D. Yang, Chem. Commun., 2008, 6182-6184
- 9. A. Choudhury, Sens. Actuator B-Chem., 2009, 138, 318-325.
- R. K. Joshi, F. E. Kruis, O. Dmitrieva, J. Nanopart. Res., 2006, 8, 797-808.
- 11. A. Cabot, J. Arbiol, J.R. Morante, U. Weimar, N. Bârsan, W. Göpel, Sens. Actuator B-Chem., 2000, 70, 87-100.
- M. Yuasaa, T. Masaki, T. Kida, K. Shimanoe, N. Yamazoea, Sens. Actuator B-Chem., 2009, 136, 99-104.
- K. I. Bolotin, K. J. Sikes, Z. Jiang, M. Klima, G. Fudenberg, J. Hone, P. Kim, H. L. Stormer, *Solid State Commun.*, 2008, 146, 351-355.
- M. Gautam, A. H. Jayatissa, Mater. Sci. Eng. C-Mater. *Biol. Appl.*, 2011, 31, 1405-1411.
- S. Srivastava, K. Jain, V. N. Singh, S. Singh, N. Vijayan, N. Dilawar, G. Gupta, T. D. Senguttuvan, *Nanotechnology*, 2012, 23, 205501-205507.
- A. M. Taurino, S. Capone, A. Boschetti, T. Toccoli, R. Verucchi, A. Pallaoro, P. Siciliano, S. Iannotta, Sens. Actuators B, 2004, 100, 177-184.
- 17. M. Gao, R. H. Hill, J. Mater. Res., 1998, 13, 1379-1389.
- Y.-J. Choi, H.-H. Park, S. Golledge, D. C. Johnson, H. J. Chang, H. Jeon, Surf. Coat. Technol., 2010, 205, 2649-2653.
- 19. P. J. Cumpson, J. Eelctron. Spectrosc., 1995, 73, 25-52.
- D. Yang, A. Velamakanni, G. Bozoklu, S. Park, M. Stoller, R.D. Piner, S. Stankovich, I. Jung, D.A. Field, C.A. Ventrice Jr., R.S. Ruoff, *Carbon*, 2009, 47, 145-152.

- 21. O. Akhavan, Carbon, 2011, 49, 11-18.
- D. Szczuko, J. Werner, S. Oswald, G. Behr, K. Wetzig, *Appl. Surf. Sci.*, 2001, 179, 301-306.
- M. D'Arienzo, L. Armelao, A. Cacciamani, C. M. Mari, S. Polizzi, R. Ruffo, R. Scotti, A. Testino, L. Wahba, F. Morazzoni, *Chem. Mater.*, 2010, 22, 4083-4089.
- K. Omura, P. Veluchamy, M. Tsuji, T. Nishio, M. Murozono, J. *Electrochem. Soc.*, 1999, 146, 2113-2116; Y.-J. Choi, H.-H. Park, *Thin Solid Films*, 2011, 519, 6214-6218.
- 25. Çetin Kılıç, Alex Zunger, Phys. Rev. Lett., 2002, 88, 095501.
- R. W. J. Scott, S. M. Yang, N. Coombs, G. A. Ozin, D. E. Williams, *Adv. Funct. Mater.*, 2003, 13(3), 225-231.
- H. Kim, S. J. Wang, H.-H. Park, H. J. Chang, H. Jeon, R. H. Hill, *Thin Solid Films*, 2007, 516, 198-202.
- H. Kim, M. K. Yun, H.-H. Park, Phys. Status Solidi A, 2011, 208, 1869-1872.
- H. Zhang, P. Xu, G. Du, Z. Chen, K. Oh, D. Pan, Z. Jiao, *Nano Res.*, 2011, 4, 274-283
- S. Chang, M. Li, Q. Hua, L. Zhang, Y. Mac, B. Ye, W. Huang, J. Catal., 2012, 293, 195-204.
- 31. H. Kim, Y.-J. Choi, Y.-H. Kim, H.-H. Park, Surf. Coat. Technol., 2013, 231, 385-388.
- 32. G. Rodriguez-Gattorno, D. Diaz, L. Rendon, G.O. Hernandez-Segura, *J. Phys. Chem., B*, 2002, 106, 2482-2487.
- H. Zengin, W. Zhou, J. Jin, R. Czerw, D.W. Smith Jr., L. Echegoyen,
 D.L. Carroll, S.H. Foulger, J. Ballato, Adv. Mater., 2002, 14,
 1480-1483